AIAA JOURNAL
Vol. 42, No. 2, February 2004

Shape Optimization of Surface Ships in Potential Flow Using an Adjoint Formulation

Saad A. Ragab*
Virginia Polytechnic Institute and State University, Blacksburg, Virginia 24061-0219

A numerical method for shape optimization of surface ships is presented. The classical potential flow theory is used, and the free surface boundary conditions are linearized using Dawson's method (see Nakos, D., and Sclavounos, P., "Ship Motions by a Three-Dimensional Rankine Panel Method," *18th Naval Hydrodynamic Symposium*, National Academy Press, Washington, DC, 1990, pp. 21–40). Objective functionals for wave resistance minimization and inverse problems are considered. An important contribution of this work is the formulation of a continuous adjoint approach for computing the gradients of these objective functionals. The potential flow problem is solved with an existing panel code (SWAN-v2.2). Like the velocity potential function, the adjoint function is governed by Laplace's equation; however, the adjoint radiation condition demands that waves may exist only upstream. The adjoint problem is also solved using the same code (SWAN-v2.2) after some modifications are introduced to handle the respective boundary conditions. Geometric characteristics, wave resistance, and surface wave patterns of optimized hull forms are presented.

Nomenclature

B	=	waterline beam
C_B	=	block coefficient
Fr	=	Froude number
$\mathcal{F}$	=	cost function; Eqs. (6–9)
f, g	=	integrand in cost function; Eq. (9)
G	=	hull geometry
g_0	=	gravitational acceleration
H	=	surface metric coefficient; Eq. (10)
L	=	ship length, reference length
$\mathcal{L}$	=	Lagrangian; Eq. (11)
m, n	=	B-spline control points indices
$\mathbf{n}$	=	unit normal to hull surface
p, P	=	pressure, P is equal to $(p - p_\infty)/\rho$
R_p	=	coefficient of wave resistance by pressure integration
R_w	=	coefficient of wave resistance by wave-cut method
S	=	hull surface area
T	=	draft
U_∞	=	freestream velocity, reference velocity
$\tilde{U}, \tilde{V}, \tilde{W}$	=	contravariant velocity components
V	=	hull volume
x, y, z	=	Cartesian coordinates
α, β, γ	=	Lagrange multipliers
η_0	=	wave elevation
θ, θ_i	=	hull geometric parameters
κ	=	g_0/U_∞^2
ξ, η	=	curvilinear coordinates
ρ	=	fluid density
ϕ	=	disturbance velocity potential
ψ	=	adjoint function

Subscripts

B	=	bow
d	=	target or design condition
$d10, d20$	=	10 and 20 design cycles
S	=	stern
0	=	baseline hull
∞	=	freestream

Received 15 February 2002; revision received 31 May 2003; accepted for publication 2 September 2003.

*Professor, Department of Engineering Science and Mechanics; ragab@vt.edu. Member AIAA.

I. Introduction

GRADIENT-BASED optimization techniques such as conjugate gradient and quasi-Newton methods, for example, that of Vanderplaats,[1] are commonly used because of their efficiency. An important step in their implementation is an accurate and fast evaluation of the gradient of the cost functional. A finite difference method can be used, but it becomes very inefficient if the number of design variables is large because it requires solving the field equations as many times as the number of design variables just to obtain the gradient. Alternatively, an adjoint approach, for example, that applied by Pironneau,[2] Jameson,[3] Baysal and Eleshaky,[4] and Soemarwoto,[5] avoids this difficulty by treating the field equations as constraints on the variations in flow variables (the velocity potential). The constrained problem is then solved by the use of Lagrange multipliers, which are defined so that the first variation of the Lagrangian with respect to flow variables vanishes.

The new contributions of this paper are the formulation of the continuous adjoint problem for free-surface flows and its implementation in a panel code for the hydrodynamic design of surface ships, as well as for bodies submerged near a free surface. The method has been applied successfully to several examples of submerged bodies[6,7] and surface ships. A baseline hull is first defined. At a given Froude number and certain geometric constraints, the hull is optimized for minimum wave resistance or for a prescribed pressure distribution on hull. The accuracy and efficiency of the adjoint approach are demonstrated by comparisons with direct calculations of the gradients with a finite difference method. Results also include geometric characteristics, wave resistance, and surface wave patterns of optimized hull forms.

II. Adjoint Formulation for Free-Surface Flow

A. Potential Flow Problem

We consider a ship in a steady rectilinear motion with constant velocity in a calm sea. Figure 1 defines a coordinate system that is fixed in the ship. The plane $z = 0$ coincides with the undisturbed free surface, and the plane $y = 0$ is assumed to be a plane of symmetry for the ship and flowfield. We linearize the free-surface conditions using either Kelvin's or Dawson's method. In this section, we use Kelvin's linearization and present modifications due to Dawson's linearization afterward. The body surface is parameterized by a set

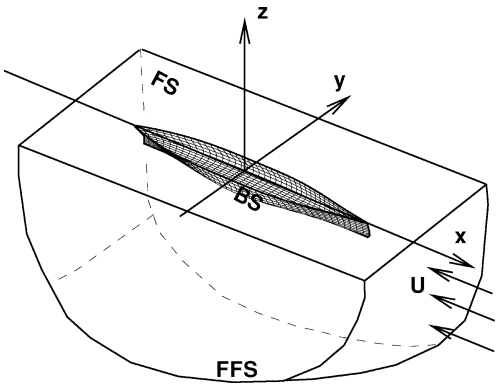

Fig. 1 Flow domain boundaries: FS, BS, and FFS.

of geometric parameters θ_i, $i = 1, \ldots, N$; in the following, we will use θ to denote any of the members of the set. In terms of the disturbance velocity potential ϕ, the flowfield is governed by the following for Ω, the body surface (BS), the free surface (FS), and the far-field surface (FFS):

$$\nabla^2\phi = 0 \qquad \text{in} \qquad \Omega \tag{1}$$

$$B(\theta, \phi) = \frac{\partial\phi}{\partial n} + \mathbf{U}_\infty \cdot \mathbf{n} = 0 \tag{2}$$

on BS,

$$M(\theta, \phi) = \frac{\partial^2\phi}{\partial x^2} + \kappa\frac{\partial\phi}{\partial z} = 0 \tag{3}$$

on FS, and

$$A(\theta, \phi) = \phi = 0 \tag{4}$$

on FFS, where $\kappa = g_0/U_\infty^2$. A radiation (uniqueness) condition that allows no waves to propagate upstream must also be added to the preceding equations.[8] We write such a condition as ϕ and

$$\frac{\partial\phi}{\partial x} \to 0 \qquad \text{as} \qquad x \to +\infty \tag{5}$$

Panel methods solve this problem very efficiently. An existing code (SWAN-v2.2) developed by Nakos and Sclavounos[9] is used to solve for the velocity potential and other flow variables.

B. Objective Functionals

A candidate objective functional is the wave resistance:

$$\mathcal{F} = \int_{\text{BS}} -pn_x \,\mathrm{d}S \tag{6}$$

where n_x is the x component of the unit normal. Another method for computing wave resistance follows from global conservation of linear momentum,[10] which is also the basis for the wave-cut method,

$$\mathcal{F} = \frac{1}{2}\rho\int_{WS}\left[-\left(\frac{\partial\phi}{\partial x}\right)^2 + \left(\frac{\partial\phi}{\partial y}\right)^2 + \left(\frac{\partial\phi}{\partial z}\right)^2\right]\mathrm{d}S + \frac{1}{2}\rho g_0\int_{-\infty}^{\infty}\eta_0^2\,\mathrm{d}y \tag{7}$$

where *WS* is a vertical plane in the far wake normal to the ship's velocity and η_0 is the wave elevation relative the undisturbed free surface. A second choice for the objective functional corresponds to an inverse problem. We seek a hull geometry whose surface pressure distribution is as near as possible to a prescribed (target) pressure. In the least-squares sense, the objective functional is given by

$$\mathcal{F} = \int_{\text{BS}} \frac{1}{2}(p - p_d)^2\,\mathrm{d}S \tag{8}$$

where p_d is the target pressure distribution. In this paper, an objective functional of the general form

$$\mathcal{F} = \int_{\text{BS}} f(\theta, \phi)\,\mathrm{d}S + \int_{\text{FS}} g(\theta, \phi)\,\mathrm{d}S \tag{9}$$

is considered, where f and g are given functions of θ and ϕ. The function g should be defined so that the free-surface integral exists. The case in which f or g is a function of pressure will be considered afterward.

C. Adjoint Problem

We assume that the hull surface and the free surface each can be mapped into a rectangular domain (ξ, η), and we express the surface element by

$$\mathrm{d}S = H(\xi, \eta, \theta)\,\mathrm{d}\xi\,\mathrm{d}\eta \tag{10}$$

The problem of minimizing $\mathcal{F}$ with respect to θ while ϕ still satisfies the respective constraints can be replaced by unconstrained minimization of a Lagrangian $\mathcal{L}$ defined by

$$\mathcal{L} = \int_{\text{BS}} f\,\mathrm{d}S + \int_{\text{FS}} g\,\mathrm{d}S + \int_{\Omega}\psi\nabla^2\phi\,\mathrm{d}\Omega + \int_{\text{BS}}\beta B\,\mathrm{d}S + \int_{\text{FS}}\gamma M\,\mathrm{d}S + \int_{\text{FFS}}\alpha A\,\mathrm{d}S \tag{11}$$

where ψ, β, γ, and α are Lagrange multipliers (also called costates or adjoint variables) that are defined on Ω, BS, FS, and FFS, respectively. The radiation condition Eq. (5), which is also a constraint on ϕ, is not included in the Lagrangian. Therefore, an admissible variation $\delta\phi$ must satisfy this condition. Observing that the Lagrangian is a sum of integrals each of the general form

$$\int G(\theta, \phi)$$

we write the variation in $\mathcal{L}$ due to a variation in θ as

$$\delta\mathcal{L} = \Sigma\int\left.\frac{\partial G}{\partial\phi}\right|_\theta\delta\phi + \Sigma\int\left.\frac{\partial G}{\partial\theta}\right|_\phi\delta\theta \tag{12}$$

The first term in Eq. (12) is undesirable because it requires $\delta\phi$. This term can be eliminated if we define the Lagrange multipliers so that

$$\Sigma\int\left.\frac{\partial G}{\partial\phi}\right|_\theta\delta\phi = 0 \tag{13}$$

and obtain

$$\frac{\mathrm{d}\mathcal{L}}{\mathrm{d}\theta} = \Sigma\int\left.\frac{\partial G}{\partial\theta}\right|_\phi \tag{14}$$

The idea is to impose sufficient conditions on ψ, β, γ, and α such that the integrals in Eq. (13) vanish. The following conditions are sufficient to eliminate all integrals except the free surface integral:

$$\nabla^2\psi = 0 \tag{15}$$

in Ω,

$$\frac{\partial\psi}{\partial n} = \frac{\partial f}{\partial\phi} \tag{16}$$

on BS,

$$\beta = -\psi \tag{17}$$

on BS,

$$\psi = 0 \tag{18}$$

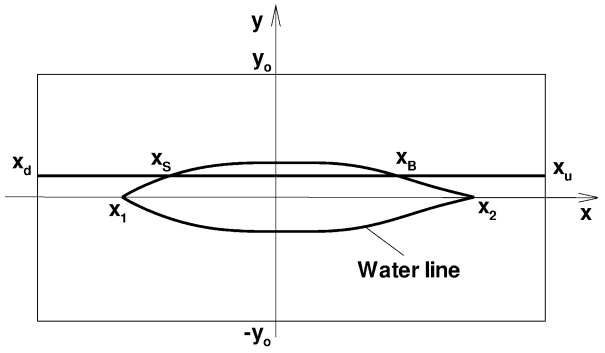

Fig. 2 FS boundaries and waterline.

on FFS, and

$$\alpha = \frac{\partial \psi}{\partial n} \tag{19}$$

on FFS. Also,

$$\gamma = -\psi/\kappa \tag{20}$$

on FS where $z = 0$. The free-surface integral reduces to

$$I_{\mathrm{FS}} = \int_{\mathrm{FS}} \left(\frac{\partial g}{\partial \phi}\delta\phi - \delta\phi \frac{\partial \psi}{\partial z} - \frac{\psi}{\kappa}\frac{\partial^2 \delta\phi}{\partial x^2} \right) \mathrm{d}S \tag{21}$$

We show in Fig. 2 a rectangular domain that covers the undisturbed free surface, and we depict the waterline where the body pierces that surface. A line parallel to the x axis may intersect the waterline at two pints $x_B(y)$ and $x_S(y)$, where B and S signify bow and stern, respectively. If the line does not intersect the waterline, we take $x_B = x_S$. We write the free-surface integral as

$$I_{\mathrm{FS}} = \int_{-y_0}^{y_0} \mathrm{d}y \int_{x_d}^{x_u} \mathrm{d}x \left(\frac{\partial g}{\partial \phi}\delta\phi - \delta\phi \frac{\partial \psi}{\partial z} - \frac{\psi}{\kappa}\frac{\partial^2 \delta\phi}{\partial x^2} \right) \tag{22}$$

where x_d and x_u are x coordinates of the downstream and upstream boundaries of a rectangular domain that covers the free surface and $-y_0$ and y_0 are its boundaries in the y direction. Integrating the last term by parts, we obtain

$$\begin{aligned} I_{\mathrm{FS}} = {} & \int_{\mathrm{FS}} \delta\phi \left(\frac{\partial g}{\partial \phi} - \frac{\partial \psi}{\partial z} - \frac{1}{\kappa}\frac{\partial^2 \psi}{\partial x^2} \right) \mathrm{d}S \\ & - \int_{-y_0}^{y_0} \frac{1}{\kappa} \left(\psi \frac{\partial \delta\phi}{\partial x} - \delta\phi \frac{\partial \psi}{\partial x} \right) \Bigg|_{x_d}^{x_u} \mathrm{d}y \\ & - \int_{-b}^{b} \frac{1}{\kappa} \left(\psi \frac{\partial \delta\phi}{\partial x} - \delta\phi \frac{\partial \psi}{\partial x} \right) \Bigg|_{x_B}^{x_S} \mathrm{d}y \end{aligned} \tag{23}$$

where b is half the maximum beam.

We get rid of the first integral by specifying the free-surface boundary condition on ψ to be

$$\frac{\partial^2 \psi}{\partial x^2} + \kappa \frac{\partial \psi}{\partial z} = \kappa \frac{\partial g}{\partial \phi} \tag{24}$$

on FS where $z = 0$. In the second integral, we invoke the radiation condition Eq. (5), which requires that $\delta\phi$ and $\partial\delta\phi/\partial x$ both be zero as $x_u \to +\infty$. Hence, the integrand of the second integral in Eq. (23) vanishes at x_u without imposing any conditions on ψ, that is, ψ and $\partial\psi/\partial x$ are unconstrained on the upstream boundary. At the downstream boundary, ϕ and $\partial\phi/\partial x$ are not constrained because waves may propagate out of the domain across that boundary. Therefore, we impose two conditions on ψ at the downstream boundary:

$$\psi \to 0, \qquad \frac{\partial \psi}{\partial x} \to 0 \qquad \text{as} \qquad x_d \to -\infty \tag{25}$$

This is a radiation condition to be satisfied by the adjoint function ψ. It implies that, for the adjoint problem, waves may exist on the upstream boundary but not downstream.

Because the velocity potential ϕ is unconstrained on the waterline, the third integral in Eq. (23) vanishes if we set $\psi = \partial\psi/\partial x = 0$ on the waterline. In this paper, we use $\psi = 0$ if the slope of the waterline is small, otherwise a natural spline condition in the direction transverse to the waterline is used. This approximate treatment works very well for ships with block coefficients less than or equal 0.63, and it requires minor modifications in the SWAN-v2.2 code, which is used for the ϕ problem.

D. Alternative Forms of the Cost Functional

Here we consider the case where f is a function of pressure $P[=(p - p_\infty)/\rho]$, which is determined from Bernoulli's equation as

$$P = \tfrac{1}{2}U_\infty^2 - \tfrac{1}{2}V^2 - g_0 z \tag{26}$$

It can be shown[11] that the boundary condition on ψ is

$$\frac{\partial \psi}{\partial n} = \frac{1}{H}\left[\frac{\partial}{\partial \xi}\left(H\tilde{U}\frac{\partial f}{\partial P} \right) + \frac{\partial}{\partial \eta}\left(H\tilde{V}\frac{\partial f}{\partial P} \right) \right] \tag{27}$$

on BS. For the objective functionals (6) and (8), we find $\partial f/\partial P$ to be $-\rho n_x$ and $\rho(P - P_d)$, respectively. The cost functional (7) that gives the wave resistance as an integral on a yz plane in the ship's wake is more reliable than integration of the pressure on the hull surface. We have formulated the adjoint problem for this cost functional. It is given by Eqs. (15), (16), (18), (24), and (25) with homogeneous conditions on BS and FS ($f = 0$ and $g = 0$) but with nonhomogeneous conditions on the downstream plane WS:

$$\psi = \frac{-\rho\partial\phi}{\partial x}, \qquad \frac{\partial \psi}{\partial x} = \frac{-\rho\partial^2\phi}{\partial x^2}$$

E. Gradient $\mathrm{d}\mathcal{L}/\mathrm{d}\theta$

After solving the adjoint problem and determining the Lagrange multipliers, we can evaluate the gradient $\mathrm{d}\mathcal{L}/\mathrm{d}\theta$:

$$\begin{aligned} \frac{\mathrm{d}\mathcal{L}}{\mathrm{d}\theta} = {} & \int_{\mathrm{BS}} \left(\frac{1}{H}\frac{\partial f H}{\partial \theta} - \psi \frac{\partial B}{\partial \theta} \right) \mathrm{d}S \\ & + \int_{\mathrm{FS}} \left(\frac{1}{H}\frac{\partial g H}{\partial \theta} - \frac{\psi}{\kappa}\frac{\partial M}{\partial \theta} \right) \mathrm{d}S \end{aligned} \tag{28}$$

This is the desired result. It can be shown that $\partial M/\partial\theta = 0$ on the free surface. More details are given by Ragab.[6]

F. Dawson's Linearized Free-Surface Condition

In the Dawson's formulation of the ship problem, the basis flow, around which the free-surface conditions are linearized, is the double-body flow. Nakos and Sclavounos[9] provide a rigorous treatment of the double-body linearization, and their formulation for steady waves is used in this section. The velocity potential is decomposed into three components: the incoming uniform stream $-U_\infty x$, the double-body disturbance potential $\bar{\phi}$, and the steady wave potential ϕ_w. The sum of the first two potentials gives the double-body flow. Two problems are solved in succession. The first is for $\bar{\phi}$, where the no-penetration condition is enforced on the hull surface BS and the undisturbed free surface FS as if it were rigid. Next, the ϕ_w problem is solved with a linearized free-surface condition whose coefficients now depend on the double-body solution $\bar{\phi}$. The double-body solution also appears as a nonhomogeneous term in the hull surface boundary conditions. It appears that two adjoint problems are needed; one for $\bar{\phi}$ and another for ϕ_w. Here, the linear problem for ϕ_w is rewritten in terms of the total disturbance potential $\phi = \phi_w + \bar{\phi}$. The advantage of working with ϕ is that $\bar{\phi}$ appears only in the coefficients of the free-surface condition, which is still

linear in ϕ, but it does not appear in the hull surface condition. In fact, the governing equations for ϕ are Eqs. (1), (2), (4), and (5) and the free-surface condition is

$$\bar{A}\frac{\partial^2\phi}{\partial x^2}+\bar{B}\frac{\partial^2\phi}{\partial y^2}+\bar{C}\frac{\partial^2\phi}{\partial x\partial y}+\bar{D}\frac{\partial\phi}{\partial x}+\bar{E}\frac{\partial\phi}{\partial y}+g_0\frac{\partial\phi}{\partial z}-\bar{F}=0 \tag{29}$$

on FS, where $z=0$. The coefficients depend on $\bar{\phi}$ only. (More details are given in Ref. 6.) The double-body disturbance potential $\bar{\phi}$ does not appear explicitly anywhere in the governing equations of the total disturbance potential ϕ, except in the coefficients of the free-surface condition Eq. (29). Therefore, a perturbation in geometry produces variations $\delta\phi$ and $\delta\bar{\phi}$, the second of which affects only the mentioned coefficients. The need to solve an adjoint equation for the double-body potential is avoided when variations in the coefficients of the free-surface condition are neglected. With this approximation in mind, the derivation presented for the Kelvin's free-surface condition can be repeated for the double-body linearization. The adjoint problem is still defined by Eqs. (15), (16), (18), (24), and (25) except that the free-surface condition (24) is now replaced by

$$\frac{\partial^2\bar{A}\psi}{\partial x^2}+\frac{\partial^2\bar{B}\psi}{\partial y^2}+\frac{\partial^2\bar{C}\psi}{\partial x\partial y}-\frac{\partial\bar{D}\psi}{\partial x}-\frac{\partial\bar{E}\psi}{\partial y}+g_0\frac{\partial\psi}{\partial z}=g_0\frac{\partial g}{\partial\phi} \tag{30}$$

on FS, where $z=0$. This condition can be adapted to the SWAN-v2.2 code.

III. Results

A. Baseline Ship G_0

A baseline ship, which is denoted by G_0, is constructed by composite B-spline surface patches. Uniform bicubic patches are used. The control points are uniformly spaced in the x and z directions, and their offsets are placed on a mathematically defined surface. However, this surface is used only for the definition of G_0 and is not needed for the optimization procedure. The plane $y=0$ is a plane of symmetry, and one-half of the hull surface is parameterized by $(m+1)(n+1)$ control points. Each control point is identified by two indices (i, j), where $i=0, 1, \ldots, m$ and $j=0, 1, \ldots, n$. For later use, the two indices are combined into a one-dimensional index $k=j(m+1)+i+1$. There are $(m-2)(n-2)$ surface patches, and each patch is subdivided into a small number of panels $(m_p \times n_p)$. The total number of panels on one-half of the hull is $m_p n_p(m-2)(n-2)$. For $m=7$ and $n=11$, the B-spline control points indices are shown in Fig. 3. The first station of bow corresponds to the indices $j=1, i=1, \ldots, 6$ and the last station of stern to $j=10, i=1, \ldots, 6$. The keel corresponds to the indices $i=1$, $j=1, \ldots, 10$ and the waterline to $i=6$, $j=1, \ldots, 10$. Each patch is subdivided into $(m_p \times n_p)=(5\times 8)$ panels, which gives 73 stations and 26 waterlines, and a total of 1800 panels on one-half of the hull. Different projections of G_0 are shown in Figs. 4 and 5.

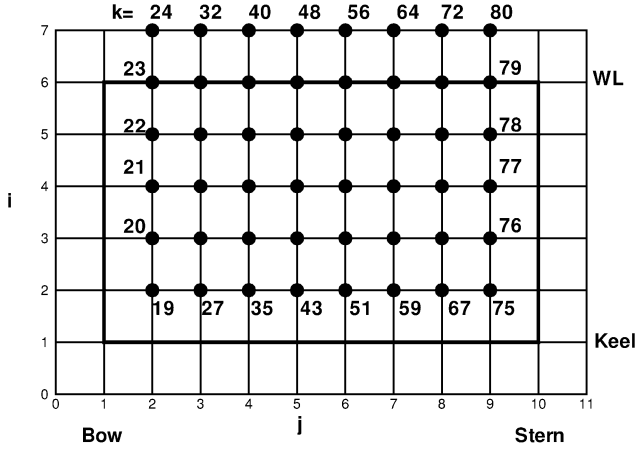

Fig. 3 Indices of B-spline control points for baseline surface ship G_0.

The ship length is used as a reference length. The first station of bow is at $x=0.5$, and the last station of stern is at $x=-0.5$. The hull is symmetric fore and aft of the midship section $(x=0)$. Some geometric characteristics of G_0 are waterline beam $B=0.116(L/B=8.62)$, draft $T=0.0544(B/T=2.13)$ (which is uniform along the ship length), displacement $V_0=0.00396$, wetted surface area $S_0=0.168$, and block coefficient $C_B=0.628$. The flow around G_0 is solved with the SWAN-v2.2 code. The basis flow around which the free-surface conditions are linearized is the double-body flow (similar to Dawson's linearization; see Ref. 9 for more details). The wave resistance coefficient as a function of Froude number (based on ship length) is shown in Fig. 6. There two curves correspond to two different methods of calculating wave resistance in SWAN-v2.2 code. The curve denoted by R_w is based on transverse wave cut method, whereas R_p is obtained by integration of surface pressure, including a waterline contribution.

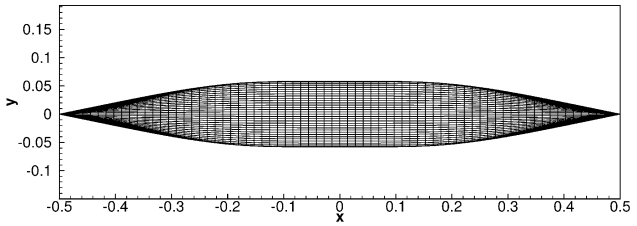

Fig. 4 Projection on the xy plane of baseline hull G_0.

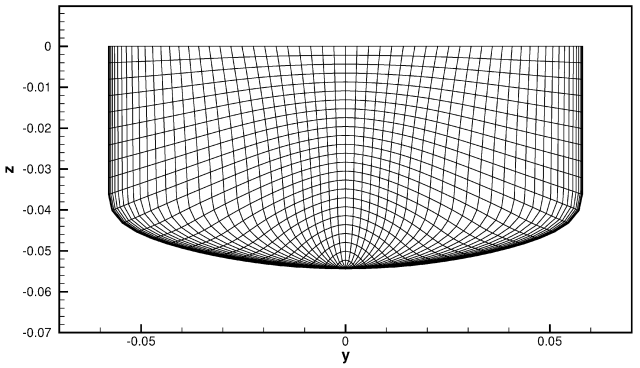

Fig. 5 Body plan of baseline hull G_0; bow $y>0$ and stern $y<0$.

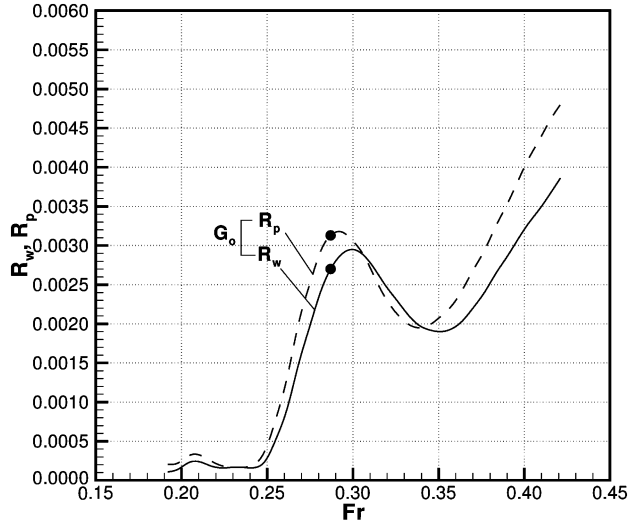

Fig. 6 Wave resistance coefficient for baseline hull G_0; R_p by pressure integration, and R_w by wave cut method.

B. Wave Resistance Minimization at Froude Number $Fr = 0.287$

The wave resistance of G_0 has a local maximum near $Fr = 0.287$ due to constructive wave interference. We choose to optimize the hull at this Froude number subject to geometric constraints. The objective functional is the wave resistance. The design variables are the offsets of the B-spline control points, whereas their depths and streamwise locations are held fixed.The number of design variables is 48 in the present example.

Because the depths and streamwise positions of the control points are fixed, the optimized hull will have a profile in the plane of symmetry the same as that of the original hull G_0. Two constraints are imposed on the optimized hull: Its displacement V_d satisfies an equality constraint $V_d = V_0$, whereas its wetted surface area S_d satisfies an inequality constraint $S_d \leq 1.3S_0$. This means that the displacement of the optimized hull is equal to that of the original hull, but its surface may be larger than the original surface. We must also specify side constraints. To this end, we let y_k^0 denote the initial values of the design variables that give the original hull G_0, and let d_1 and d_2 denote the minimum and maximum of these values, respectively. In terms of these quantities, we define lower and upper limits for each design variable: $y_k^l = \text{maximum}(d_1, 0.5y_k^0)$ and $y_k^u = \text{minimum}(1.2\,d_2, 1.5y_k^0)$. Finally, we specify the side constraints by $y_k^l \leq y_k \leq y_k^u$. This constrained optimization problem is solved with a generalized reduced gradient method (GRG) as detailed by Belegundu and Chandrupatla.[12]

Credibility of the adjoint method for computing the gradient of the cost functional with respect to the design variables y_k must be established. For this purpose, comparison is made between the gradient found by the adjoint and that by a finite difference method. In the latter method, the control variables y_k are perturbed one at a time, and the cost functional is computed on each perturbed hull. With the cost functional on the unperturbed hull known, the gradient is computed by a first-order forward finite difference method. There are 48 control variables, and thus, the flowfield has to be calculated on 48 different perturbed hulls in addition to the unperturbed one. This should be compared with only two solutions for the adjoint approach: one for the velocity potential and the other for the adjoint function. The 48 components of the gradient computed by the two methods are shown in Fig. 7 against the index k, which is defined by Fig. 3. The overall agreement between the two methods is satisfactory. The discrepancies in the components of the two gradients after normalization by the magnitude of the gradient vector are less than 6%. Comparisons between adjoint and finite difference method for other cases of surface ships and fully submerged bodies are given by Ragab.[6,7]

The reduction of the cost functional obtained by the GRG method is shown in Fig. 8. The iteration process is terminated after 20 design cycles because the reduction is deemed sufficient, whereas further reduction becomes very slow in the current GRG method. The designed hull, which is denoted by G_{d20} S287, is shown in Figs. 9 and 10. We note that the bow and stern regions are pinched, and a small bulge develops at the midship region. The stern region suffers the most modifications. The maximum waterline beam is 0.133 and the wetted surface area is 0.173, which is 3.0% larger than that of G_0. The wave resistance coefficient of G_{d20} S287 over a range of Froude numbers is compared with that of G_0 in Fig. 11. At the optimization Froude number $Fr = 0.287$, the coefficient R_w for G_0 is 0.00270, and for G_{d20} S287 it is 0.000204. The reduction in the wave resistance is approximately 92%. Recall that this result is based on potential flow theory. Also note that the wave resistance of the designed hull is lower than that of G_0 over the Froude number range 0.25–0.35. Outside this range the trend is reversed. The lower wave resistance of G_{d20} S287 manifests itself in the wave pattern and water line wave elevation shown in Figs. 12 and 13, respectively. As is evident in Fig. 13, the stern wave is significantly reduced, whereas the bow wave is slightly reduced. Note that there are two waves on the baseline hull G_0, whereas only one wave can be identified on the designed hull G_{d20} S287.

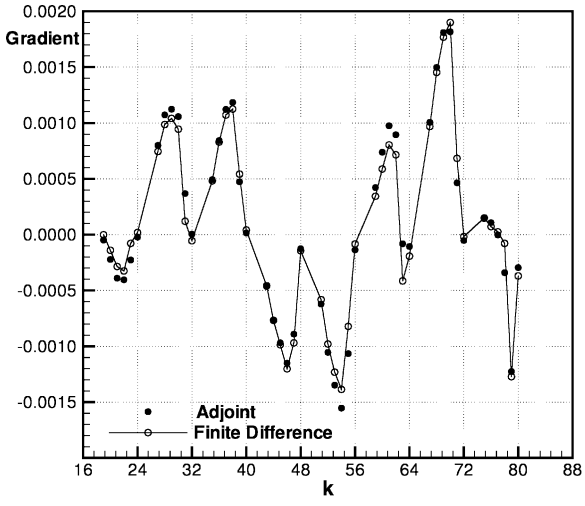

Fig. 7 Gradient of cost function computed by finite difference and adjoint methods; hull G_0, $Fr = 0.287$.

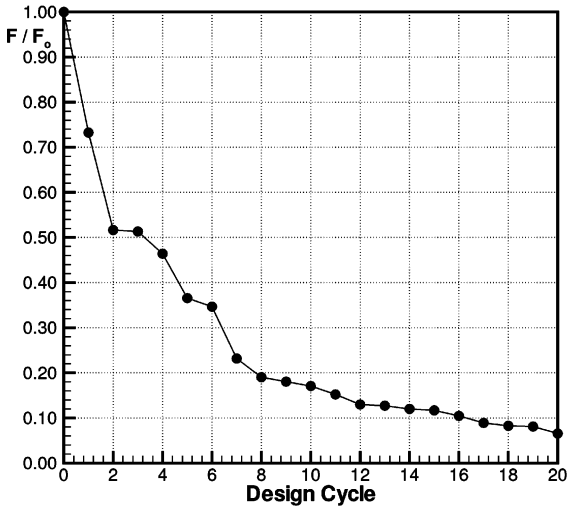

Fig. 8 Reduction of cost functional with design cycles for G_{d20} S287.

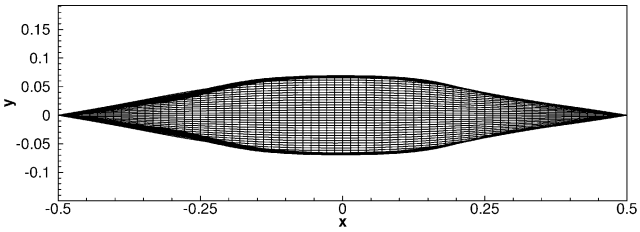

Fig. 9 Projection on the xy plane of designed hull G_{d20} S287.

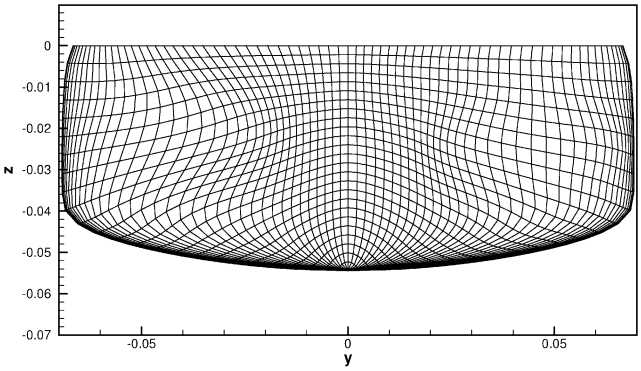

Fig. 10 Body plan of designed hull G_{d20} S287; bow $y > 0$ and stern $y < 0$.

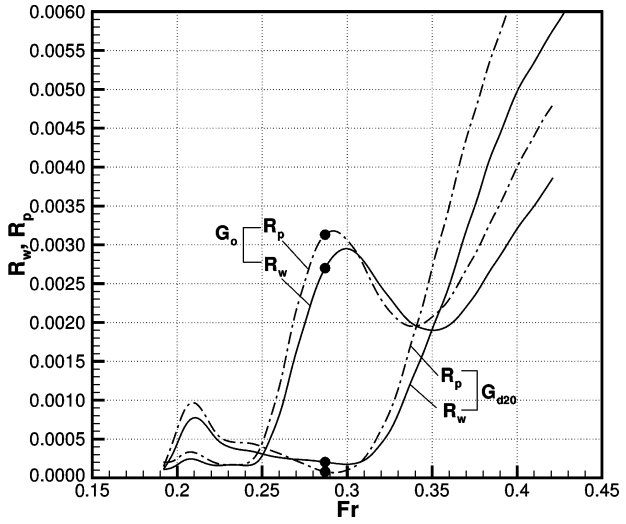

Fig. 11 Wave resistance coefficient for baseline hull G_0 and designed hull G_{d20} S287; R_p by pressure integration and R_w by wave cut method.

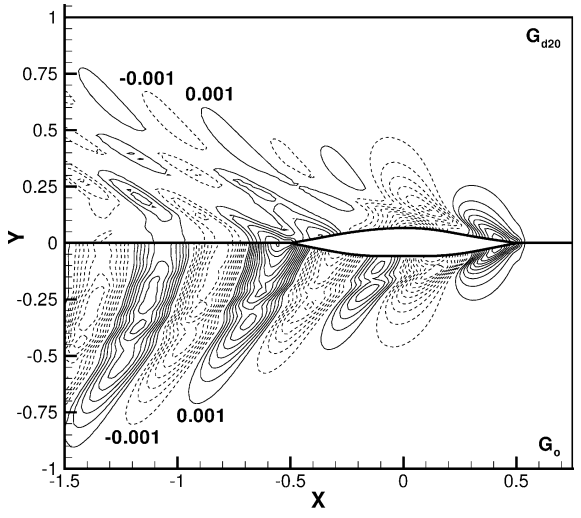

Fig. 12 Wave pattern on baseline hull G_0 (lower half) and designed hull G_{d20} S287 (upper half).

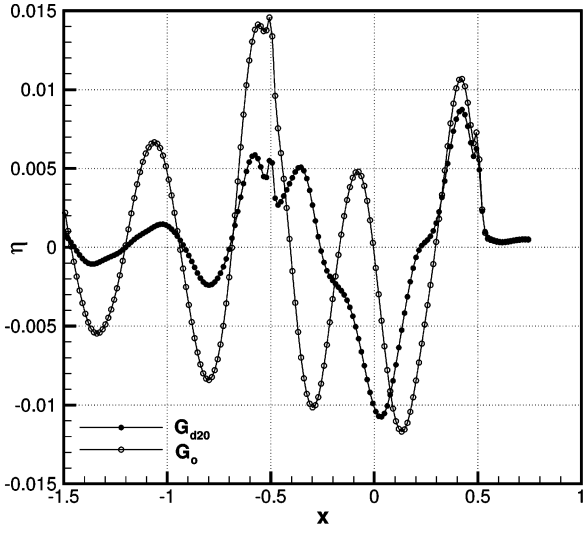

Fig. 13 Waterline wave elevation on baseline hull G_0 and designed hull G_{d20} S287.

C. Target Pressure Distribution at Froude Number $Fr = 0.287$

This section concerns the application of the present shape optimization method to the solution of an inverse problem in ship hydrodynamics. The objective is to design a hull form so that the pressure distribution on its surface matches a target distribution to be specified by the designer. For example, when the pressure distribution on an existing hull is first determined, the designer may choose to introduce modifications to mitigate flow separation or cavitation in a certain locality. An exact solution to the inverse problem may not exist. The use of shape optimization techniques provides a hull form whose pressure distribution is as near as possible to the target distribution.

To demonstrate the method, the target pressure distribution is given by the double-body pressure coefficient distribution on the baseline hull G_0. This is an interesting target pressure because it gives zero wave drag on G_0. Although Froude number (or gravitational) effects do not play a role in the determination of the double-body pressure coefficient, the optimized hull form depends on the Froude number at which optimization is performed. Moreover, the wave drag of the designed hull may not be zero. Even though the pressure coefficient at each panel center of the optimized hull matches the target distribution, the area and orientation of each panel may have been changed from those of the corresponding panel of G_0. The double-body pressure distribution gives zero drag only on G_0, but not necessarily on a deformed shape that follows from it.

The inverse problem is solved at Froude number $Fr = 0.287$. The constraints on displacement and wetted surface area, as well as side constraints, are exactly the same as given in Sect. III.B. After 10 design cycles, the target and actual pressure distributions on the designed hull G_{d10} are shown in Fig. 14 as a function of x at four different depths. Figure 14a, at $k_z = 1$, corresponds to the row of panels closest to the free surface, and Fig. 14d, at $k_z = 25$, corresponds to the last row of panels at the keel. The pressure distribution on the baseline hull G_0 at Froude number $Fr = 0.287$ is given by the dashed line. This pressure distribution is significantly different from the double-body pressure distribution on the same hull (shown by the open circles), which is used as a target pressure. It is evident in Fig. 14 that the pressure on the optimized hull is close to the target pressure almost everywhere on the hull, except in the bow region ($x = 0.5$) near the waterline ($k_z = 1$). This is expected because shape deformation downstream of bow has little influence on bow flow due to the hyperbolic character of the free-surface condition.

The designed hull, which is denoted by G_{d10} S287P, is shown in Figs. 15 and 16. It is observed that the bow region is strongly pinched, but the stern suffers less modifications. The maximum waterline beam is 0.127, and the wetted surface area is 0.172, which is 2.3% larger than that of G_0. The body plan depicted in Fig. 16 shows that the hull lacks symmetry fore and aft of the midship section.

The optimization iteration is continued for another 20 cycles, but no changes are observed in optimized hull form. The wave resistance coefficient over a range of Froude number is shown in Fig. 17. At the design Froude number $Fr = 0.287$, the wave drag coefficient is $R_w = 0.000907$; thus, the drag reduction is 65% of the baseline hull. Although the objective functional in this example is for a target pressure, the wave resistance of the designed hull shows favorable reduction over relatively high Froude numbers up to 0.4. This is because the target pressure corresponds to a case where there is no wave resistance.

D. Sensitivity Study

In general, numerical designs such as the one presented here have two sources of uncertainties. The first arises from the basic assumptions inherent in the mathematical model. In this work, the optimized hull forms are based on the potential flow theory with linearized free-surface boundary conditions. The mathematical derivation of the associated adjoint problem is exact. Therefore, there are uncertainties due to neglecting viscous effects and nonlinearities in the free-surface boundary condition. To estimate these uncertainties, one needs to optimize the hull forms by adopting the Navier–Stokes

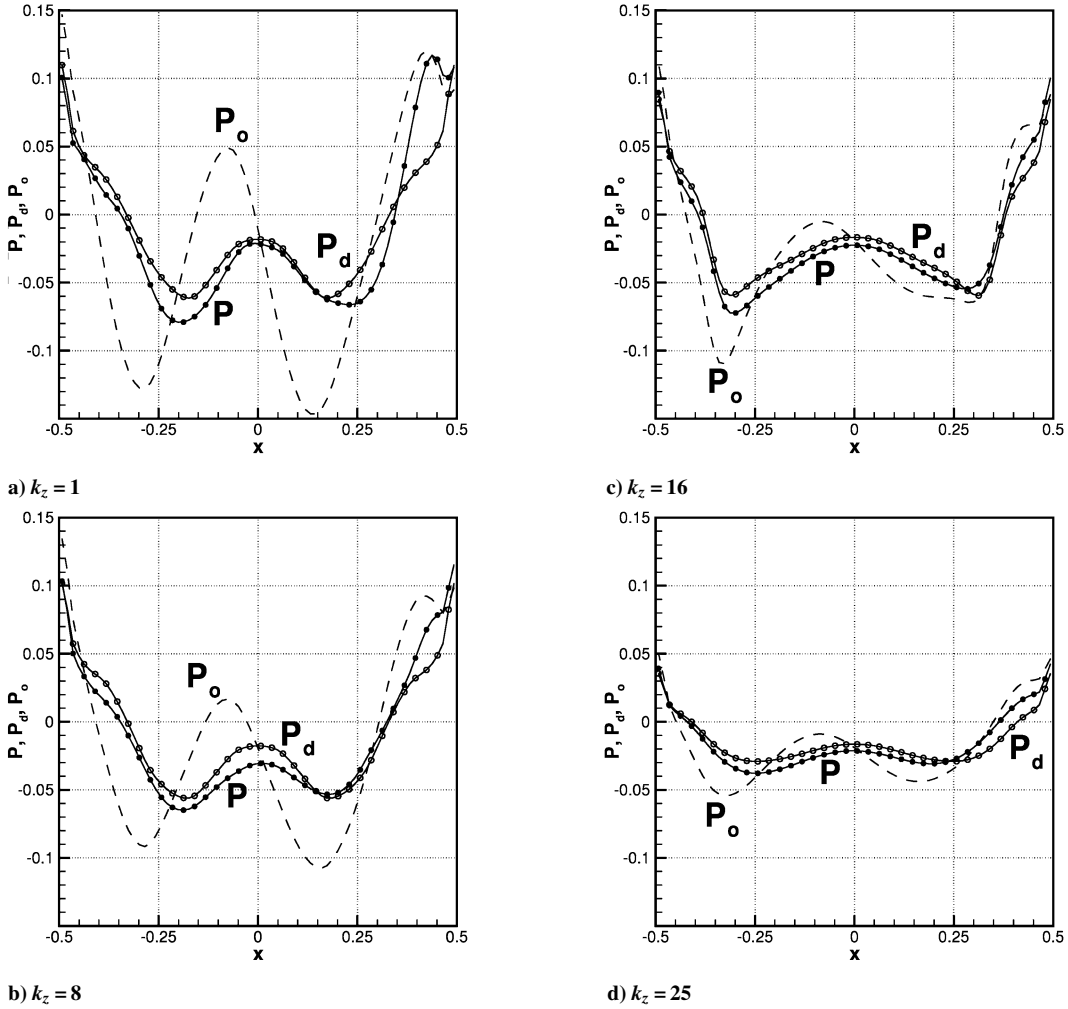

Fig. 14 Pressure distribution on hull: P = pressure on designed hull G_{d10} S287P, P_d = target pressure, and P_0 = pressure on G_0, $Fr = 0.287$.

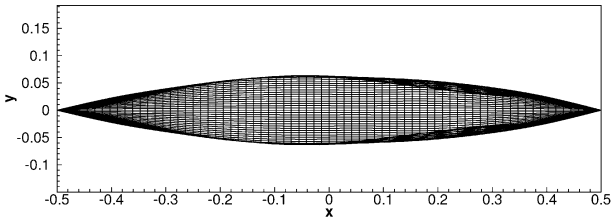

Fig. 15 Projection on the xy-plane of designed hull G_{d10} S287P.

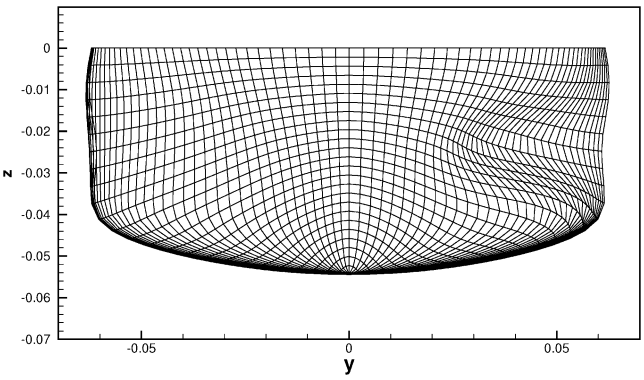

Fig. 16 Body plan of designed hull G_{d10} S287P; bow $y > 0$ and stern $y < 0$.

equations as a mathematical model with nonlinear free-surface conditions. This is an important problem by itself, especially for the near-field disturbances and friction and form drag. Its solution is very expensive and would require significant computing resources. The radiated waves and wave resistance, which constitute the subject of this paper, are essentially inviscid phenomena. Hull forms based on inviscid models, even though they may suffer from uncertainties due to neglecting viscous effects, are inexpensive to obtain and represent good candidates for improvement by optimization based on more exact models such as the Navier–Stokes equations.

The second source of uncertainties is introduced by errors in the numerical treatment of the different components of the mathematical model. In this work, these errors are introduced as a result of replacing the continuous inviscid flow problem and its adjoint by discrete finite dimension problems. To estimate the uncertainties arising from these errors, we use two measures of sensitivity, namely, the geometric characteristics of the hull forms and their performance. This is achieved by investigation of the effects of grid resolution on these measures. We consider the designs presented in Secs. III.B and III.C as reference designs for the respective cost functions and refer to them as case 0. In these designs, each B-spline surface patch is divided into 40 panels, giving a total of 1800 panels on one-half of the hull. To determine the effects of the number of panels, we use finer and coarser grids, namely, 54 and 28 panels per patch, giving, respectively, a total of 2430 and 1260 panels on one-half of the hull. These cases will be referred to as cases 1 and 2, respectively. All other design parameters are kept the same as in

Table 1 Sensitivity study of designed hull G_{d20} S287

Parameter	Case 0[a]	Case 1	Case 2	Case 3	Case 4
Input					
Number of panels per patch	40	54	28	40	40
Number of design cycles	20	20	20	30	20
Paneled free surface area	0.75	0.75	0.75	0.75	0.60
Output					
Waterline beam $= 0.129 + \cdots$	——	$0.10E{-}2$	$-0.20E{-}2$	$0.30E{-}2$	$0.10E{-}2$
Waterline area $= 0.0793 + \cdots$	——	$-0.17E{-}2$	$-0.19E{-}2$	$-0.52E-2$	$-0.09E{-}2$
$R_w(Fr = 0.287) = 0.343 \times 10^{-3} + \cdots$	——	$-0.12E{-}4$	$-0.33E{-}4$	$0.27E{-}4$	$-0.20E{-}4$
$R_w(Fr = 0.383) = 0.343 \times 10^{-2} + \cdots$	——	$0.20E{-}3$	$-0.30E{-}4$	$0.31E{-}4$	$0.16E{-}3$

[a]Reference design.

Table 2 Sensitivity study of designed hull G_{d20} S287P

Parameter	Case 0[a]	Case 1	Case 2	Case 3	Case 4
Input					
Number of panels per patch	40	54	28	40	40
Number of design cycles	10	10	10	20	10
Paneled free surface area	0.75	0.75	0.75	0.75	0.60
Output					
Waterline beam $= 0.124 + \cdots$	——	$-0.20E{-}2$	$0.00E{-}0$	$0.00E{-}0$	$0.00E{-}0$
Waterline area $= 0.0836 + \cdots$	——	$-0.60E{-}3$	$0.10E{-}3$	$0.30E{-}3$	$0.00E{-}0$
$R_w(Fr = 0.287) = 0.950 \times 10^{-3} + \cdots$	——	$0.24E{-}4$	$-0.20E{-}4$	$-0.44E{-}4$	$-0.80E{-}5$
$R_w(Fr = 0.383) = 0.229 \times 10^{-2} + \cdots$	——	$-0.20E{-}4$	$-0.40E{-}4$	$-0.60E{-}4$	$0.30E{-}4$

[a]Reference design.

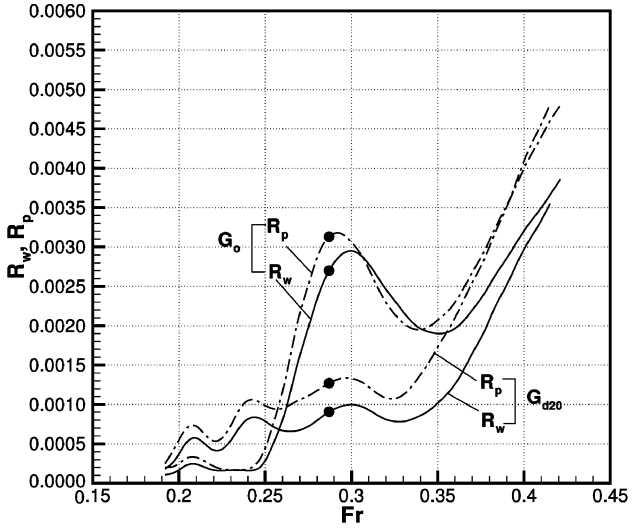

Fig. 17 Wave resistance coefficient for baseline hull G_0 and designed hull G_{d20} S287P; R_p by pressure integration and R_w by wave cut method.

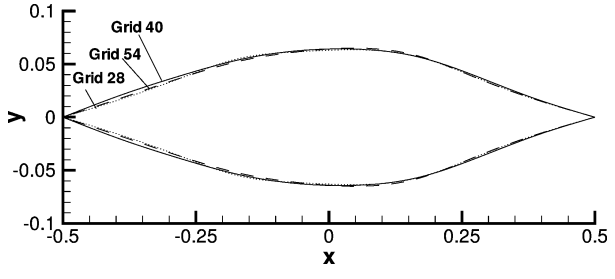

Fig. 18 Sensitivity of waterline of designed hull G_{d20} S287 to grid resolution: ——, reference grid; · · · ·, coarse grid; and – – –, fine grid.

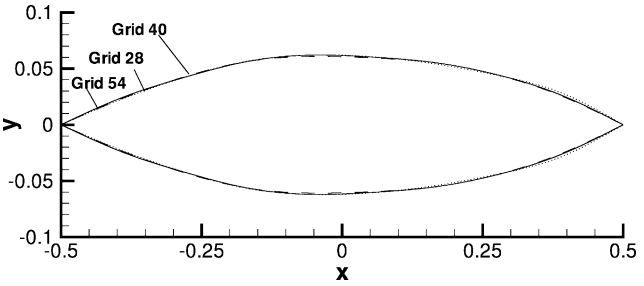

Fig. 19 Sensitivity of waterline of designed hull G_{d10} S287P to grid resolution: ——, reference grid; · · · ·, coarse grid; and – – –, fine grid.

case 0. The waterlines of the three cases are shown in Fig. 18 for the minimum wave resistance design and in Fig. 19 for the prescribed surface pressure design. For clarity, the y-axis scale is exaggerated by a factor of two relative to the x-axis scale. Aside from negligible changes in the stern region of the minimum wave resistance hull, the results show that the optimized hulls are independent of grid resolution. The effects of these geometric changes on the hull performance (the wave resistance coefficient) are shown in Tables 1 and 2, for the two designs, respectively. Tables 1 and 2 show the sensitivities in the waterline beam, waterline area, and wave resistance coefficients R_w at the design Froude number of 0.287 and at an off-design number of 0.383. Also shown in Tables 1 and 2 are sensitivities due to the number of design cycles (case 3) and the size of paneled area on the free surface (case 4). Again, these sensitivities are small.

IV. Conclusions

An efficient gradient-based optimization method has been applied successfully to the hydrodynamic design of surface ships. The efficiency of the method stems from the use of an adjoint formulation for the gradient of the cost functional with respect to design variables. The flow model is given by the classical potential flow theory with Kelvin's or Dawson's linearized free-surface condition. A baseline hull is first defined. This hull is optimized for minimum wave resistance or for a target pressure distribution subject to constraints on displacement and surface area. The constrained problem is solved

by a generalized reduced gradient method. B-spline surfaces are used for geometry parameterizations and prove to be versatile for shape optimization.

The accuracy of the adjoint formulation has been validated by comparisons with direct calculations with a finite difference method. In all examples considered, the discrepancies between the two methods is less than 6% of the gradient vector magnitude. Furthermore, the geometric characteristics and hydrodynamic performance of an optimized hull with a finite difference method used to calculate gradient (not shown in this paper) have been compared with that calculated with the adjoint approach. Although there are differences in the geometric details of the two hull forms, they show an almost identical wave pattern and wave resistance, not only at the optimization Froude number $Fr = 0.287$, but also over a wide range of Froude numbers. This is because the two hull forms have equal sectional area distributions.

The current GRG methods takes about 20, or less, design cycles to reach a minimum. All of the adjoint results presented in this work have been obtained on a fine grid of 7800 panels (1800 panels on one-half of the hull). Computations have been performed on a single-processor SGI-R10000 workstation. Typical wall times to complete 20 design cycles are 48–72 h. A finite difference method would take an estimated 700–1000 h on the same grid and for the same number of design variables.

Acknowledgments

This work has been supported by the U.S. Office of Naval Research under Grant N00014-98-1-0843. The author thanks Arthur Reed and John Telste (U.S. Naval Surface Warfare Center, Carderock Division), for their help with the interpretation of results and providing technical support with the SWAN-v2.2 code.

References

[1]Vanderplaats, G. N., *Numerical Optimization Techniques For Engineering Design*, 2nd ed., Vanderplaats Research and Development, Inc., Colorado Springs, CO, 1998, Chap. 6.

[2]Pironneau, O., *Optimal Shape Design for Elliptic Systems*, Springer-Verlag, New York, 1984.

[3]Jameson, A., "Aerodynamic Design via Control Theory," *Journal of Scientific Computing*, Vol. 3, 1988, pp. 233–260.

[4]Baysal, O., and Eleshaky, M. E., "Aerodynamic Design Optimization Using Sensitivity Analysis and Computational Fluid Dynamics," *AIAA Journal*, Vol. 30, No. 3, 1992, pp. 718–725.

[5]Soemarwoto, B., "The Variational Method for Aerodynamic Optimization Using the Navier–Stokes Equations," ICASE Rept. 97-71, 1997; also NASA CR-97-206277, 1997.

[6]Ragab, S. A., "Shape Optimization in Free Surface Potential Flow Using an Adjoint Formulation," U.S. Naval Surface Warfare Center, Carderock Div., NSWCCD-50-TR-2003/33, Bethesda, MD, Aug. 2003.

[7]Ragab, S. A., "An Adjoint Formulation for Shape Optimization in Free-Surface Potential Flow," *Journal of Ship Research*, Vol. 45, No. 4, 2001, pp. 269–278.

[8]Stoker, J. J., *Water Waves*, Interscience, New York, 1957, pp. 174, 209.

[9]Nakos, D., and Sclavounos, P., "Ship Motions by a Three-Dimensional Rankine Panel Method," *18th Naval Hydrodynamic Symposium*, National Academy Press, Washington, DC, 1990, pp. 21–40.

[10]Wehausen, J. V., "The Wave Resistance of Ships," *Advances in Applied Mechanics*, Vol. 13, 1973, pp. 93–245.

[11]Ragab, S. A., "Hydrodynamic Design of Three-Dimensional Nonlifting Surfaces," American Society of Mechanical Engineers, Paper FEDSM97-3414, June 1997.

[12]Belegundu, A. D., and Chandrupatla, T. R., *Optimization Concepts and Applications in Engineering*, Prentice–Hall, Upper Saddle River, NJ, 1999, pp. 176–181.

P. R. Bandyopadhyay
Associate Editor